THE JOURNAL OF BIOLOGICAL CHEMISTRY VOL. 289, NO. 30, pp. 20727–20739, July 25, 2014

The Mechanism of Dynein Light Chain LC8-mediated Oligomerization of the Ana2 Centriole Duplication Factor*

Received for publication, April 23, 2014, and in revised form, May 30, 2014 Published, JBC Papers in Press, June 11, 2014, DOI 10.1074/jbc.M114.576041

Lauren K. Slevin[‡1], **Erin M. Romes**[§1], **Mary G. Dandulakis**[‡], **and Kevin C. Slep**[‡2]

From the Departments of [‡]*Biology and* [§]*Biochemistry and Biophysics, University of North Carolina, Chapel Hill, North Carolina 27599*

Background: Ana2 is a conserved centriole duplication factor involved in nascent centriole biogenesis.
Results: Two sites in the central domain of Ana2 (Ana2M) bind LC8 and form an $Ana2M_4$-$LC8_8$ complex.
Conclusion: LC8 potentiates Ana2 tetramerization.
Significance: LC8-potentiated Ana2 tetramerization is expected to increase the avidity of Ana2 for centriole factors, including Sas-6, and may drive binding factor oligomerization.

Centrioles play a key role in nucleating polarized microtubule networks. In actively dividing cells, centrioles establish the bipolar mitotic spindle and are essential for genomic stability. *Drosophila* anastral spindle-2 (Ana2) is a conserved centriole duplication factor. Although recent work has demonstrated that an Ana2-dynein light chain (LC8) centriolar complex is critical for proper spindle positioning in neuroblasts, how Ana2 and LC8 interact is yet to be established. Here we examine the Ana2-LC8 interaction and map two LC8-binding sites within the central region of Ana2, Ana2M (residues 156–251). Ana2 LC8-binding site 1 contains a signature TQT motif and robustly binds LC8 (K_D of 1.1 μM), whereas site 2 contains a TQC motif and binds LC8 with lower affinity (K_D of 13 μM). Both LC8-binding sites flank a predicted ~34-residue α-helix. We present two independent atomic structures of LC8 dimers in complex with Ana2 LC8-binding site 1 and site 2 peptides. The Ana2 peptides form β-strands that extend a central composite LC8 β-sandwich. LC8 recognizes the signature TQT motif in the first LC8 binding site of Ana2, forming extensive van der Waals contacts and hydrogen bonding with the peptide, whereas the Ana2 site 2 TQC motif forms a uniquely extended β-strand, not observed in other dynein light chain-target complexes. Size exclusion chromatography coupled with multiangle static light scattering demonstrates that LC8 dimers bind Ana2M sites and induce Ana2 tetramerization, yielding an $Ana2M_4$-$LC8_8$ complex. LC8-mediated Ana2 oligomerization probably enhances Ana2 avidity for centriole-binding factors and may bridge multiple factors as required during spindle positioning and centriole biogenesis.

Centrioles are cylindrical cellular structures that form the core of centrosomes and basal bodies, organelles responsible for nucleating polarized microtubule networks in the cytoplasm and cilia, respectively. A cell's centriole count largely determines its capabilities, because single centrioles form the base of sensory cilia, whereas multiple centrioles are needed to nucleate motile cilia (1). A centriole pair constitutes the core of the centrosome, needed for bipolar mitotic spindle formation. Centriole structure is largely conserved across metazoans, protists, and some plants, with a characteristic 9-fold radial symmetry established by an inner, 9-spoked cartwheel structure (2). Although different species have different microtubule arrangements in the surrounding blades (singlets, doublets, or triplets, as shown in Fig. 1*A*) as well as different cartwheel architectures (3), the critical centriole duplication components are conserved. The inner cartwheel recruits centriolar proteins and pericentriolar matrix components to build and elongate the outer centriole wall. During elongation, nine sets of microtubule blades (each a microtubule triplet in the case of *Drosophila*) form around the centriole perimeter parallel to the longitudinal axis, propagating the organelle's 9-fold radial symmetry.

Canonical centriole duplication is coupled to the cell cycle to limit centriole number (4). A subset of conserved centriole proteins are involved in centriole duplication (5), because their misregulation leads to increased or decreased centriole counts (Fig. 1*B*). Three key initiation factors include Polo-like kinase 4 (Plk4), spindle assembly abnormal protein 6 (Sas-6), and anastral spindle 2 (Ana2/STIL/Sas-5, found in *Drosophila melanogaster*, humans, and *Caenorhabditis elegans*, respectively). Plk4 is a serine/threonine kinase whose catalytic activity is required for centriole duplication. Plk4 phosphorylates a set of both known and unknown components to transmit the centriole duplication signal (6, 7). Plk4 is recruited to the centriole through an interaction with Asterless (Asterless/Cep-152 found in *D. melanogaster* and humans, respectively), but the conserved definitive target of the Plk4 kinase activity remains unknown (7). Downstream of Plk4, nascent centriole construction involves Sas-6 oligomerization to form the inner, 9-fold symmetric cartwheel (8–10). A third and less studied centriole-

* This work was supported, in whole or in part, by National Institutes of Health Grants R01GM094415 (to K. C. S.) and T32GM008570 (to the University of North Carolina Program in Molecular and Cellular Biophysics). This work was also supported by a National Science Foundation Graduate Research Fellowship under Grant DGE-0646083 (to L. K. S.).
The atomic coordinates and structure factors (codes 4QH7 and 4QH8) have been deposited in the Protein Data Bank (http://wwpdb.org/).
[1] Both authors contributed equally to this work.
[2] To whom correspondence should be addressed: Dept. of Biology, 402 Fordham Hall, Campus Box 3280, University of North Carolina, Chapel Hill, NC 27599-3280. Tel.: 919-962-4858; Fax: 919-962-1625; E-mail: kslep@bio.unc.edu.

initiating factor is the Sas-6-binding protein, Ana2, whose role in centriole duplication is unclear.

Ana2 was identified in a genome-wide screen in which Ana2 depletion caused a decrease in centriole count (11). Ana2 is functionally conserved across metazoan species, with orthologs in humans (STIL), *Danio rerio* (STIL), and *C. elegans* (SAS-5) (12). However, the Ana2 sequence has diverged among species, with similarity restricted to an N-terminal Sas-4 binding site (13, 14), a central predicted coiled-coil, and a C-terminal STAN (STil/ANa2) domain that binds Sas-6 *in vitro* (12, 15, 16) (Fig. 1*C*; see domain conservation presented in the *inset*, scored using percentage identity and percentage similarity between species). In *Drosophila* oocytes, Sas-6 overexpression results in centriole amplification only when Ana2 is dually overexpressed (17). In human systems, expression of Ana2 is essential in maintaining centriole count (18). Furthermore, mutations in Ana2 have been linked to primary microcephaly, leukemia, and cancer (19–23). How Ana2 and Sas-6 synergistically function remains to be determined. Although the function of Ana2 is poorly understood, recent work has demonstrated that *Drosophila* Ana2 interacts with the dynein light chain, LC8 (cut up (Ctp)) (24), a ubiquitous protein that binds diverse targets throughout the cell to confer or potentiate target dimerization (reviewed in Ref. 25). The Ana2-LC8 interaction is important for directing spindle orientation during *Drosophila* larval brain development (Fig. 1*D*). Loss of either Ana2 or LC8 results in aberrant spindle positioning and defective separation of apicobasal polarity determinants during neuroblast asymmetric cell division.

Although LC8 acts as a processivity factor for the dynein motor by enhancing motor dimerization, it largely plays a dynein motor-independent role throughout the cell to potentiate dimerization of its binding partners (26–37). It was shown in a yeast two-hybrid screen that LC8 binds two Ana2 fragments: the first fragment spanning residues 1–200 and the second spanning residues 201–274, which includes a predicted α-helix highly conserved across fly species (Fig. 1, *E* and *F*) (24, 12). To date, there is no structural insight into the LC8-Ana2 complex.

Here, we use x-ray crystallography, isothermal microtitration calorimetry (ITC),[3] and size exclusion chromatography with multiangle static light scattering (SEC-MALS) to characterize the interactions between LC8 and Ana2. Our results demonstrate that LC8 dimers bind Ana2 at two distinct sites, the first of which contains a high-affinity, canonical LC8-binding TQT motif (residues 159–168), whereas the second contains a non-canonical TQC motif (residues 237–246). We present the structures of LC8 bound to peptides encompassing both of the LC8 binding sites of Ana2 as well as the apo-LC8 dimer and highlight the conserved Ana2 features that underlie these different interactions with the peptides. SEC-MALS analysis of WT and mutant Ana2M (residues 156–251) in complex with LC8 reveals LC8-dependent Ana2M tetramerization in an $Ana2M_4$-$LC8_8$ complex. The Ana2 LC8 binding sites flank a predicted α-helix probably involved in Ana2 oligomerization. Our findings suggest that LC8 is responsible for enhancing Ana2 oligomerization and structural stability. LC8-potentiated Ana2 oligomerization has spatial and avidity implications for the Ana2 N-terminal Sas-4 binding motif and its C-terminal Sas-6-binding STAN domain.

EXPERIMENTAL PROCEDURES

Cloning and Expression of Full-length LC8—Full-length *D. melanogaster* LC8 was subcloned into the pGEX-6P-2 expression vector (GE Healthcare). pGEX-6P-2-LC8 was transformed into *E. coli* BL21 DE3 (pLysS) and grown under ampicillin selection in 6 liters of LB medium at 37 °C. At an optical density of 0.6 (600 nm), GST-LC8 expression was induced using 0.1 mM isopropyl-1-thio-β-D-galactopyranoside for 16 h at 18 °C. Cells were harvested by centrifugation at 2100 × *g* for 10 min at 4 °C, and the pellets were resuspended in buffer A (25 mM Tris, pH 8.0, 300 mM sodium chloride, and 0.1% β-mercaptoethanol) and stored at −20 °C.

Protein Purification for Crystallization—LC8 was purified as described previously for the yeast homologue Dyn2 (29). Briefly, cells expressing GST-LC8 were lysed by sonication and clarified by centrifugation at 23,000 × *g* for 45 min, and the supernatant was loaded onto a Glutathione Sepharose column (GE Healthcare). The column was washed with buffer A, and the GST-LC8 fusion was eluted in buffer A supplemented with 25 mM glutathione. The GST tag was cleaved with PreScission protease (GE Healthcare). LC8 was subsequently purified on an SP Sepharose Fast Flow column (GE Healthcare) and exchanged into MES storage buffer (25 mM MES, pH 6.0, 50 mM sodium chloride, and 0.1% β-mercaptoethanol). LC8 was concentrated to 0.5 mM, snap frozen in liquid nitrogen, and stored at −80 °C. The final LC8 contains an N-terminal five-residue (GPLGS) cloning artifact.

Synthesis of Ana2 Peptides—Ana2 peptides were synthesized at the UNC Microprotein Sequencing and Peptide Synthesis Facility, and lyophilized peptides were reconstituted in final MES storage buffer. An N-terminal, non-native Asn and Tyr were added to each peptide to facilitate peptide concentration determination (underlined in the sequences presented below). The Ana2 peptide sequences are peptide 1 (pep1) (NYTICAGTQTDP (Ana2 residues 159–168)) and peptide 2 (pep2) (NYSSTTGTQCDI (Ana2 residues 237–246)).

Crystallization of the LC8-Ana2 Peptide Complexes—Final concentrations of 0.5 mM LC8 and 0.6 mM Ana2 pep1 (or 0.75 mM LC8 and 0.9 mM Ana2 pep2) in MES storage buffer were incubated for 30 min on ice. For the LC8-pep1 complex, crystallization followed the hanging drop protocol using 2 μl of the LC8/Ana2 pep1 mixture and 2 μl of a 1-ml well solution that contained 0.3 M magnesium acetate, 0.1 M sodium cacodylate, pH 6.5, and 26% (w/v) polyethylene glycol 8000. The same method was used for LC8-pep2 in a well solution containing 0.19 M ammonium acetate, 27% (w/v) polyethylene glycol 4000, 0.1% β-mercaptoethanol, and 0.1 M sodium acetate, pH 4.6. For both structures, crystals grew at 20 °C into rods (pep1) or rounded cubes (pep2) within 3 days and remained at full size for

[3] The abbreviations used are: ITC, isothermal microtitration calorimetry; DIC, dynein intermediate chain; SEC-MALS, size exclusion chromatography with multiangle static light scattering; pep1 and pep2, peptide 1 and 2, respectively.

up to 3 weeks. Crystals were transferred into fomblin oil (Sigma) cryoprotectant and flash frozen in liquid nitrogen.

Data Collection, Structure Determination, and Refinement—Diffraction data were collected on LC8-Ana2 crystals (both peptides) at the Advanced Photon Source SER-CAT beamline 22-ID with 1° oscillations over 180° from single crystals. Data were indexed, integrated, and scaled using HKL2000 (38). The LC8-Ana2 peptide structures were determined using the AutoMR molecular replacement program (PHENIX crystallographic suite (39)) and a modified 2PG1 (36) coordinate file in which a monomeric (for LC8-Ana2 pep1) or dimeric (for LC8-Ana2 pep2) apo-*Drosophila* LC8 search model was used. The models were built using AutoBuild (PHENIX) and refined iteratively through manual builds in Coot (40), followed by refinement runs using phenix.refine against a maximum likelihood target (PHENIX) (39). Refinement statistics were monitored using a free *R*, calculated using 5.4 or 5.6% of the data for pep1 and pep2, respectively, randomly excluded from refinement (41).

Isothermal Microtitration Calorimetry—ITC experiments were carried out at 26 °C in MES storage buffer on a MicroCal AutoITC200 (GE Healthcare). Lyophilized peptides were solubilized in MES storage buffer. 19 2-μl injections of 1.0 mM Ana2 pep1 were automatically injected into 200 μl of 50 μM LC8, and 2.0 mM pep2 was automatically injected into 200 μl of 100 μM LC8. The resulting binding isotherms were analyzed using the Origin version 7.0 software package (OriginLab) and were fit to a single-site, independent binding model. Ana2 peptide control experiments were performed to determine the contribution from each peptide's heat of dilution. These controls involved 19 2-μl injections of 1.0 mM Ana2 pep1 or 2.0 mM Ana2 pep2 into a chamber containing 200 μl of MES storage buffer. The Ana2 pep1 control isotherm did not reveal significant heat of dilution; therefore, the final five injection values (where binding was saturated in the pep1-LC8 isotherm) were averaged, and this value was subtracted from each injection in the pep1-LC8 experiment. The Ana2 pep2 control isotherm revealed a significant endothermic heat of dilution (data not shown); therefore, these control values were individually subtracted from the corresponding raw experimental values from the pep2-LC8 binding isotherm. Experiments were conducted in triplicate, the internal or external controls were subtracted, and the resulting heats of dilution were averaged to determine respective mean K_D and S.D. values.

Cloning and Expression of LC8 and Ana2M Constructs for SEC-MALS—Full-length *D. melanogaster* LC8 was subcloned into a pET28b expression vector (EMD Millipore) with an engineered PreScission protease (GE Healthcare) cleavage site following the N-terminal His_6 tag. The subcloning of SNAP-tagged LC8 (New England Biolabs) into pET28b followed a similar protocol. *D. melanogaster* Ana2 residues Asp^{156}–Gln^{251} (Ana2M) was subcloned into a pGEX-6P-2 expression vector (GE Healthcare). pET28b-LC8 and pGEX-6P-2-Ana2M were separately transformed into *E. coli* BL21 DE3 (pLysS) and grown individually under kanamycin (LC8) or ampicillin (Ana2M) selection, each in 5 liters of LB medium at 37 °C. At an optical density of 0.6 (600 nm), His_6-LC8 or GST-Ana2M expression was induced using 0.2 mM isopropyl-1-thio-β-D-galactopyranoside for 16 h at 18 °C. Cells were harvested by centrifugation at 2100 × *g* for 10 min at 4 °C, and the pellets of both His_6-LC8 and GST-Ana2M were combined and resuspended in buffer A (25 mM Tris, pH 8.0, 10 mM imidazole, 300 mM sodium chloride, and 0.1% β-mercaptoethanol) and stored at −20 °C.

Ana2M-LC8 Complex Purification for SEC-MALS—The composite pellet of His_6-LC8 and GST-Ana2M was thawed and lysed by sonication with the addition of phenylmethanesulfonyl fluoride to a final concentration of 200 μM. The supernatant was purified over Ni^{2+}-nitrilotriacetic acid resin (Qiagen) followed by PreScission protease (GE Healthcare) treatment to cleave off the His_6 and GST tags. The LC8-Ana2M complex was subsequently purified over a Superdex 200 size exclusion column (GE Healthcare) and concentrated in SEC-MALS buffer: 25 mM HEPES, pH 7.5, 300 mM sodium chloride, 0.1% β-mercaptoethanol. The presence of both components was confirmed by SDS-PAGE. Expression and purification of the Ana2M-SNAP-LC8 complex followed a similar protocol.

Mutagenesis of Ana2M—An Ana2M site 1 LC8-binding mutant (Q165A/T166A) was created using the QuikChange (Agilent Technologies) method on the wild-type GST-Ana2M construct according to the manufacturer's instructions. The mutant GST fusion protein was expressed and co-purified with wild-type LC8 as described above.

SEC-MALS—LC8-Ana2M complexes (100 μl) were injected onto a Wyatt WTC-030S5 silicone size exclusion column (for elution of 5–1,250-kDa proteins) in SEC-MALS buffer supplemented with 0.2 g/liter sodium azide and passed in tandem through a Wyatt DAWN HELEOS II light scattering instrument and a Wyatt Optilab rEX refractometer. The light scattering and refractive index data were used to calculate the weight-averaged molar mass and the mass fraction in each peak using the Wyatt Astra V software program (Wyatt Technology Corp.) (42).

RESULTS

Ana2 Contains Two High-affinity LC8 Binding Sites—Drosophila Ana2 is a 420-residue centriole duplication component that lacks apparent conservation across species barring an N-terminal Sas-4 binding region (13, 14), a central predicted coiled-coil domain, and the highly conserved C-terminal STAN (STil/ANa2) motif (Fig. 1, *C*, *E*, and *F*) (12). Previous studies demonstrated a physical interaction between the N-terminal 274 residues of Ana2 and LC8, a dynein light chain, via yeast two-hybrid screening (24). Structure function analysis indicated that Ana2 contained at least two LC8 binding sites, one within the region spanning residues 1–200 and the second within the region spanning residues 201–274. LC8 binds many subcellular targets across species in a cytoplasmic dynein motor-independent mechanism to promote target dimerization (43), suggesting that LC8 may potentiate Ana2 oligomerization. To map the interactions between Ana2 and LC8, we scanned Ana2(1–274) for potential LC8 binding sites. LC8 target motifs comprise up to 11 contiguous residues, which, although diverse in sequence composition, often contain a $K^{-3}X^{-2}T^{-1}Q^{0}T^{1}$ or $G^{-2}I^{-1}Q^{0}V^{1}D^{2}$ motif with the conserved glutamine (Gln^{0}) set as the zero reference point (44). Target peptides with these LC8-binding motifs bind LC8 with K_D values in the 0.1–100 μM range (44, 45). We identified two poten-

tial binding sites within Ana2, corresponding to residues 159–168 (containing a $T^{-1}Q^{0}T^{1}$ sequence) and 237–246 (containing a $T^{-1}Q^{0}C^{1}$ sequence). These two sites flank either end of the conserved predicted coiled-coil (Fig. 1, *E* and *F*) and correlate with the two fragments identified via yeast two-hybrid as LC8-binding segments.

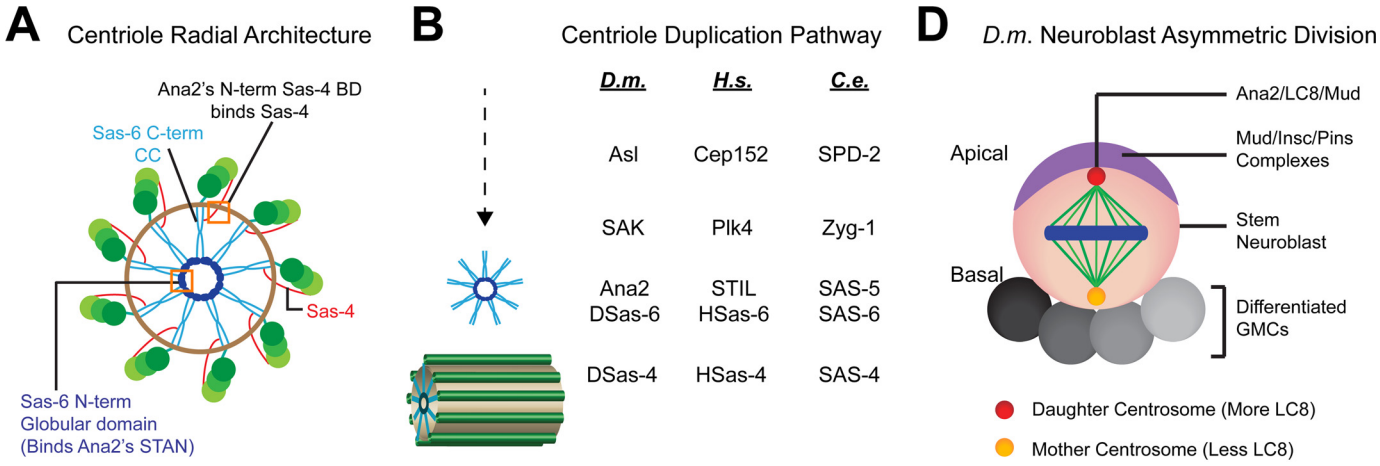

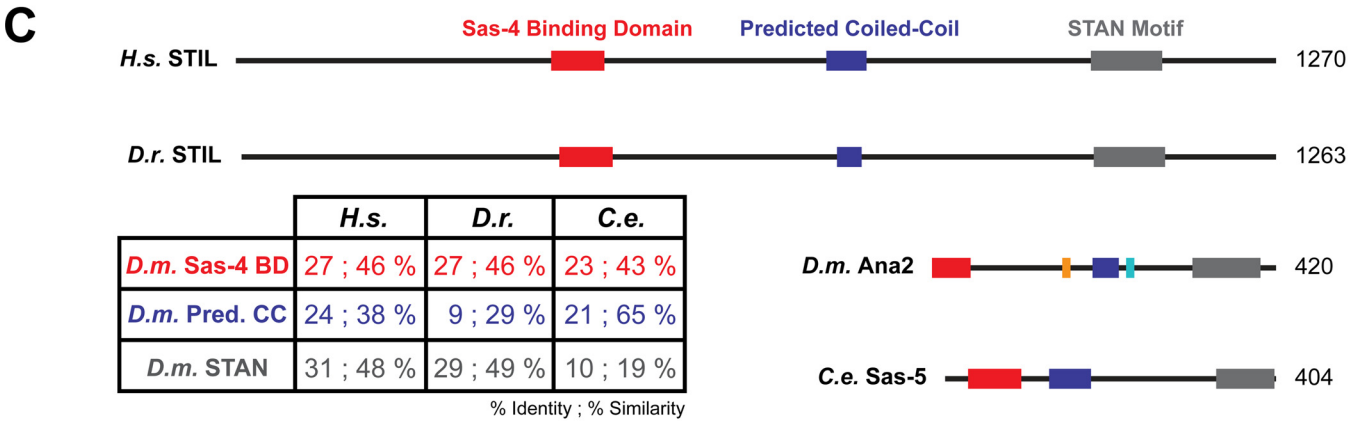

	H.s.	*D.r.*	*C.e.*
***D.m.* Sas-4 BD**	27 ; 46 %	27 ; 46 %	23 ; 43 %
***D.m.* Pred. CC**	24 ; 38 %	9 ; 29 %	21 ; 65 %
***D.m.* STAN**	31 ; 48 %	29 ; 49 %	10 ; 19 %

% Identity ; % Similarity

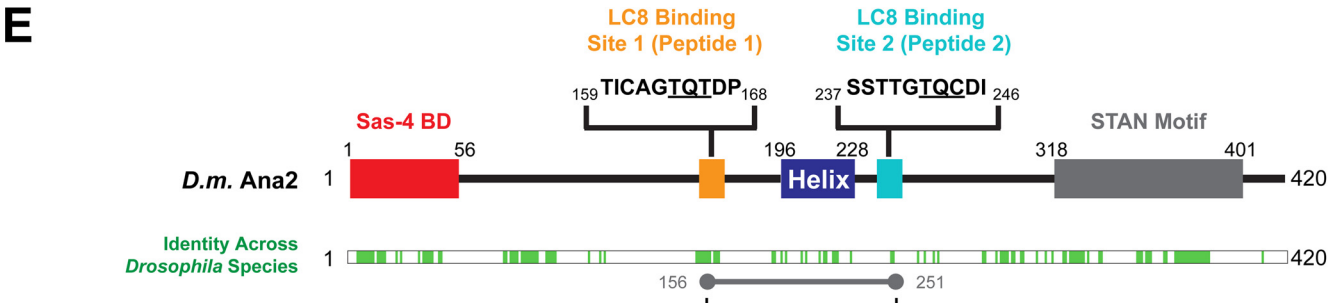

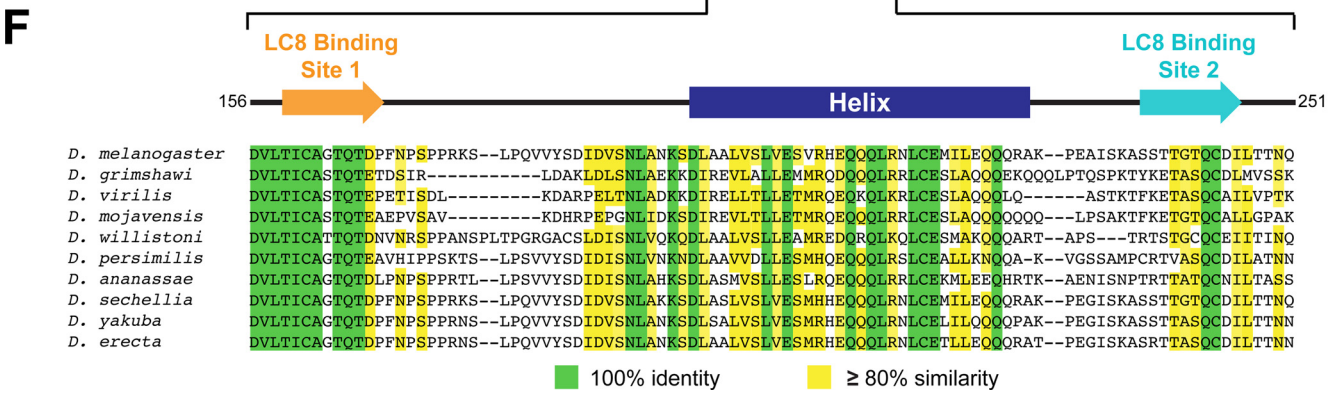

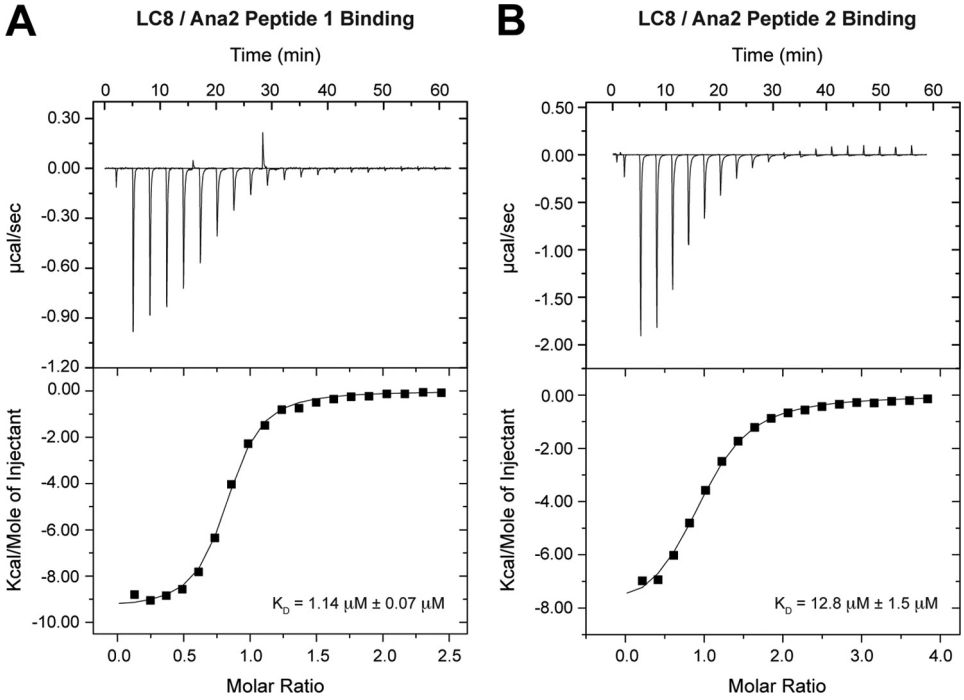

FIGURE 2. **LC8 binds two Ana2 sites with different affinities.** ITC isotherms of Ana2 peptide-LC8 interactions. *A*, 19 × 2 μl of 60 μM Ana2 peptide 1 was injected into 200 μl of 50 μM LC8. *B*, 18 × 2 μl of 2 mM Ana2 peptide 2 was injected into 200 μl of 100 μM LC8. Both Ana2 peptides display exothermic binding to LC8. The thermal profiles were integrated (*top panels* in *A* and *B*) and fit to a one-site binding model during iterative fitting until the model best fit the data. Each experiment was run in triplicate, with the K_D reported as the average (*bottom right* of *bottom panels*) with S.D. indicated.

To determine whether these sites were conserved, we aligned several Ana2 sequences from 10 different *Drosophila* species. Much of the protein is conserved within the genus, with the largest concentration of identity mapping to the STAN motif and an N-terminal region with no predicted secondary structure but involved in Sas-4 binding (Fig. 1*E*) (13, 14). Additional identity maps to the central predicted coiled-coil and the flanking regions that contain the tentative LC8-binding sites that we identified (Fig. 1*F*). The linkers that bridge the predicted LC8 binding sites with the central, predicted coiled-coil show diversity in both sequence length and composition. When we analyzed the central, predicted coiled-coil domains in Ana2 orthologs (human STIL, zebrafish STIL, and *C. elegans* Sas-5), only Sas-5 contained a potential QT motif N-terminal to the predicted coiled-coil with the sequence KTVNVSQTVE, suggesting that the LC8-Ana2 interaction may be specific to a subset of Ana2 orthologs.

To confirm the ability of the putative LC8-binding sites of Ana2 to bind LC8, we synthesized peptides corresponding to the two predicted Ana2-LC8 binding sites (Fig. 1*A*) and performed ITC, monitoring the heat released as each peptide was titrated into the calorimeter cell containing purified LC8. Experiments were performed in triplicate, with reported values reflecting the average of all trials. The Ana2 peptide 1 (pep1)-LC8 binding isotherm was exothermic and yielded a K_D value of 1.14 ± 0.07 μM (Fig. 2*A*). Compared with reported LC8-target affinities (100 – 0.1 μM) (44, 45), Ana2 pep1 binds LC8 in the higher-affinity range. The Ana2 pep2 binding isotherm was also exothermic and yielded an experimentally determined LC8 K_D value of 12.8 ± 1.5 μM (Fig. 2*B*), a weaker binding affinity than

FIGURE 1. **Ana2 contains two conserved LC8 binding sites.** *A*, the nascent centriole cartwheel with mapped components. The precise location of Ana2 on the cartwheel remains unknown, but it is known to bind the Sas-6 N-terminal region (12) and the Sas-4 C-terminal region (13). *B*, a conserved set of proteins drive centriole duplication. Conserved centriole duplication pathway components from *D. melanogaster* (*D.m.*), *Homo sapiens* (*H.s.*), and *C. elegans (C.e.*) are presented with orthologous proteins listed in the same *row*. *Drosophila* Asl (Asterless) recruits SAK/Plk4 (Polo-like kinase-4) to the site of nascent centriole formation via a direct interaction (50, 51), where it phosphorylates both a known and unknown set of substrates in the centriole duplication pathway (7, 52). Sas-6 (spindle assembly abnormal-6) oligomerizes to form the first structure observed using electron microscopy; this nine-spoked cartwheel is depicted on the *left*. In cells, Sas-6 oligomerization is Ana2 (anastral spindle-2)-dependent (9, 12, 17). Sas-4 (spindle assembly abnormal-4) is thought to recruit triplet microtubule blades and stabilize centriole elongation and maturation (mature centriole shown at the *left*) (5, 13, 14). *C*, comparison of *Homo sapiens*, *D. rerio* (*D.r.*), *D. melanogaster*, *and C. elegans* Ana2 orthologs reveals diversity in protein structure. Although the lengths of Ana2 orthologs differ, the presence of a Sas-4 binding domain (*red*), an Sas-6 binding domain (STAN domain; *gray*), and a predicted central coiled-coil region remain constant (domains shown as determined previously (12, 14)). *Inset*, alignments of individual Sas-4 binding domains and STAN domains between *D. melanogaster* and *H. sapiens*, *D. rerio*, or *C. elegans* reveal high percentages of invariant (first value) and similar (second value) residues. *D*, Ana2 and LC8 form a complex with Mud to orient the mitotic spindle during asymmetric divisions in the developing *Drosophila* neuroblast (24). Asymmetry is achieved, in part, via differential maturation of the centrosomes. The daughter centrosome forms the LC8-Ana2-Mud complex that coordinates spindle alignment with cortical polarity cues to maintain a stem population (ganglion mother cell (*GMC*)) (53, 24). *E*, full-length *Drosophila* Ana2 has an N-terminal Sas-4 binding region (13, 14) and a C-terminal STAN motif (12) conserved across functional Ana2 orthologs. The central predicted helical domain is flanked by two LC8 binding sites (site 1, residues 159–168; site 2, residues 237–246). Residue identity across *Drosophila* species is noted *below* in *green*. *F*, conservation within the Ana2 central helical domain and LC8 binding sites. Residues with 100% identity are highlighted in *green*, whereas those with 80% similarity are highlighted in *yellow*. Note that both the TQT (positions 165–166) and TQC (positions 243–244) sites are conserved within the genus.

TABLE 1
LC8-Ana2 crystallographic data, phasing, and refinement

	LC8-Ana2 peptide 1	LC8-Ana2 peptide 2/apo-LC8
Data collection		
Wavelength (Å)	1.00000	1.07426
Space group	$P2_12_12_1$	P1
Cell dimensions (Å)		
a	51.5	36.6 (α = 99.3)
b	77.9	44.8 (β = 103.0)
c	108.9	85.9 (γ = 91.8)
Resolution (Å)	50.00–1.83 (1.90–1.83)[a]	50.00–1.90 (1.97–1.90)
Reflections		
Measured	108,273	70,555
Unique	37,488	36,096
Completeness (%)	95.1 (95.2)	87.5 (47.3)
Mean redundancy	2.9 (2.5)	2.0 (1.8)
I/σ	13.7 (2.4)	19.5 (7.0)
R_{sym}[b]	0.08 (0.37)	0.04 (0.12)
Refinement		
Resolution (Å)	45–1.83 (1.87–1.83)	36–1.90 (1.95–1.90)
R/R_{free} (%)	17.6 (22.1)/20.7 (24.2)	18.5 (20.1)/23.6 (31.1)
No. of reflections, R/R_{free}	34,418/1953	33,673/1991
Total atoms	3356	4580
Protein/Water	3046/310	4320/260
Stereochemical ideality (root mean square deviations)		
Bonds/angles (Å/degrees)	0.007/0.98	0.008/1.07
Mean *B*-factors (Å^2)		
MC/SC/water	16.5/20.5/31.3	15.8/19.9/21.1
B-Factor root mean square deviation (Å^2)	3.2	4.8
Ramachandran analysis		
Favored/allowed (%)	98.1/1.9	95.7/3.9

[a] Values in parentheses are for the highest resolution shells unless otherwise denoted.
[b] $R_{sym} = \Sigma_h\Sigma_i|I_i(h) - \langle I(h)\rangle|/\Sigma_h\Sigma_i I_i(h)$, where $I_i(h)$ is the *i*th measurement and $\langle I(h)\rangle$ is the mean of all measurements of $I(h)$ for Miller indices *h*.

pep1 but within the commonly reported range of LC8-target affinities.

Crystallization of LC8 Ana2 Pep1 and Pep2 Complexes—To determine the molecular determinants underlying the LC8-Ana2 interaction, we attempted to crystallize LC8 in complex with each synthesized Ana2 peptide. Both LC8-peptide complexes were amenable to crystallization, although diffraction quality crystals formed in different conditions (see "Experimental Procedures"). Ana2 pep1-LC8 crystals diffracted to 1.83 Å resolution and belonged to the space group $P2_12_12_1$ (Table 1). Ana2 pep2-LC8 crystals diffracted to 1.9 Å resolution and belonged to the space group P1 (Table 1). To solve both structures, we performed molecular replacement using a search model containing a single *Drosophila* LC8 chain (for Ana2 pep1) or an LC8 dimer (for Ana2 pep2) without bound peptide, derived from Protein Data Bank entry 2PG1 (36).

The Structure of LC8 Bound to Ana2 Pep1—Four LC8 chains were found in the asymmetric unit. The LC8 chains are paired to form two independent homodimers, each arranged around non-crystallographic 2-fold axes. Clear electron density was evident in the initial $F_o - F_c$ map to build four Ana2 pep1 chains (Fig. 3*A*), two bound to each LC8 homodimer. The structure was built and refined to *R* and R_{free} values of 17.6 and 20.7%, respectively (see Table 1 for refinement statistics).

The LC8 homodimer forms a composite platform for Ana2 pep1 binding (Fig. 3*B*). The homodimeric core is characterized by a central 12-stranded β-sandwich, each half of which is formed by four β-strands from one LC8 chain (β1 from Val^7–Asp^{12}, β4 from His^{72}–Leu^{78}, β5 from Val^{81}–Lys^{87}, β2 from Trp^{54}–Gly^{59}), one β-strand from the LC8 homodimeric mate (β3′ from Gly$^{63'}$–Glu$^{69'}$), and the Ana2 peptide, which contributes the sixth and final β-strand (Fig. 3*B*). Each β-sheet is entirely antiparallel. The β-sandwich is flanked on either side by two α-helices. Ana2 pep1 binding engages determinants in both LC8 chains, with β3 forming a key extended interface with the peptide (Fig. 3*B*). Peptide binding is stabilized by backbone/backbone antiparallel β-sheet hydrogen bonding (Fig. 4*A*) as well as several side chain interactions. The Ana2 conserved glutamine Gln^{165} (notated as Q^0 in reference to its position in the canonical $K^{-3}X^{-2}T^{-1}Q^0T^1$ binding motif) forms key contacts, including van der Waals interactions with both LC8 chains and hydrogen bonds with the Glu$^{35'}$ side chain carboxylate group and the Lys$^{36'}$ backbone amide, serving to cap the α2′ helix's N-terminal region (Fig. 4*B*).

The Structure of LC8 Bound to Ana2 Pep2—The Ana2 pep2-LC8 crystal contains three LC8 dimers in the P1 unit cell. One LC8 dimer is bound to two Ana2 pep2 chains (Fig. 3, *A* and *C*), whereas the other two LC8 dimers are in the apo form with crystal packing sterically occluding the peptide binding sites. The structure was built and refined to *R* and R_{free} values of 18.5 and 23.7%, respectively (see Table 1 for refinement statistics).

Ana2 pep2 binds in a manner similar to Ana2 pep1, extending either side of the LC8 core β-sandwich and making several backbone interactions with LC8 β3 (Figs. 3*C* and 4*A*). Gln^0 of Ana2 pep2 participates in similar interactions as observed in the LC8-Ana2 pep1 structure; however, pep2 contains a non-canonical cysteine residue at the +1-position, Cys^{244}. To our knowledge, this is the first example of an LC8 target with a cysteine in the +1-position. In contrast to the canonical threonine at the +1-position, Ana2 pep2 Cys^{244} is angled into the

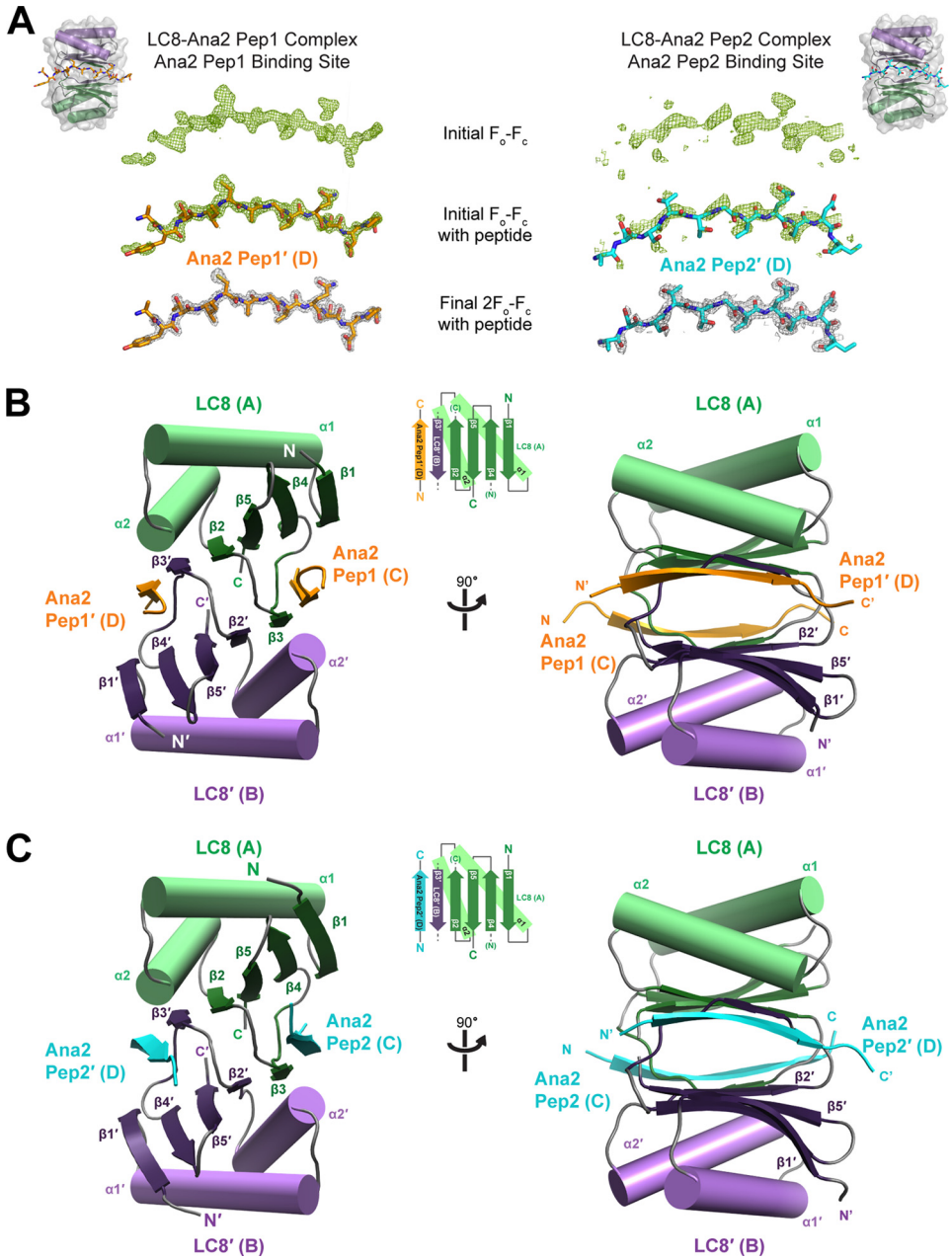

FIGURE 3. **Structures of LC8-Ana2 complexes reveal LC8 homodimers bound to two parallel Ana2 peptides.** *A*, LC8-Ana2 complex structures were determined using peptide-free LC8 search models. Initial $F_o - F_c$ electron density for the Ana2 peptides is shown in *green* and contoured at 2.0σ (pep1) and 1.65σ (pep2). Final $2F_o - F_c$ electron density is shown *below* in *gray* with the final Ana2 pep1 and pep2 model included; electron density is contoured at 2.0 σ (pep1) and 1.0 σ (pep2). Final models of the respective LC8-Ana2 peptide complexes are presented in the *top left* (LC8-Ana2 pep1) and *top right* (LC8-Ana2 pep2) with peptides in the same orientation for reference. *B* and *C*, the final structures of LC8 bound to Ana2 pep1 (*orange*; *B*) and Ana2 pep2 (*cyan*; *C*) are shown looking down the complex's 2-fold axis (*left*) and after a 90° rotation about the *y* axis (*right*). The *center schematic* in *B* and *C* summarizes the secondary structure elements that comprise a single β-sheet in the LC8-peptide complexes. Each β-sheet is extended by the third β-strand contributed by the LC8 homodimeric mate (*purple*) as well as the bound Ana2 peptide (pep1 shown in *orange* (*B*); pep2 shown in *cyan* (*D*)). The final β-sheet comprises a total of six strands and is flanked by two α-helices (shown in *mint*, *behind* the sheet).

LC8 peptide binding groove, with its side chain engaging LC8 Glu$^{35\prime}$, Arg^{60}, Asn^{61}, Phe^{62}, Tyr^{77}, and Ala^{82}. Specifically, the cysteine's terminal sulfhydryl group forms a 3.6-Å electrostatic interaction with the backbone carbonyl of LC8 Arg^{60} (Fig. 4*C*). This shift allows for extended backbone-backbone contacts, including interactions between Ana2 Cys^{244} and LC8 Phe^{62}, as well as between Ana2 Ile^{246} and LC8 Arg^{60} (Fig. 4*D*). As a result, the Ana2 pep2 C-terminal region differentially engages the LC8 dimer as compared with Ana2 pep1, whose respective determinants are positioned 3–5 Å away (Fig. 4*D*).

The LC8 Binding Pocket Undergoes Structural Shifts to Accommodate Ana2 Peptides—In addition to observing an LC8-Ana2 pep2 complex in the P1 unit cell, two sets of apo-LC8 homodimers were also present. As observed previously (45), the apo-LC8 binding pocket is narrower than the peptide-bound cleft observed in both Ana2-bound LC8 structures (Fig. 5*A*). Several LC8 residues that directly engage the Ana2 peptides are swung toward the peptide binding pocket in the apo state, including Asn^{10}, Lys$^{36\prime}$, Tyr^{65}, Thr^{67}, Phe^{73}, Tyr^{75}, and Tyr^{77}, highlighting the mobility of LC8 side chains upon target binding.

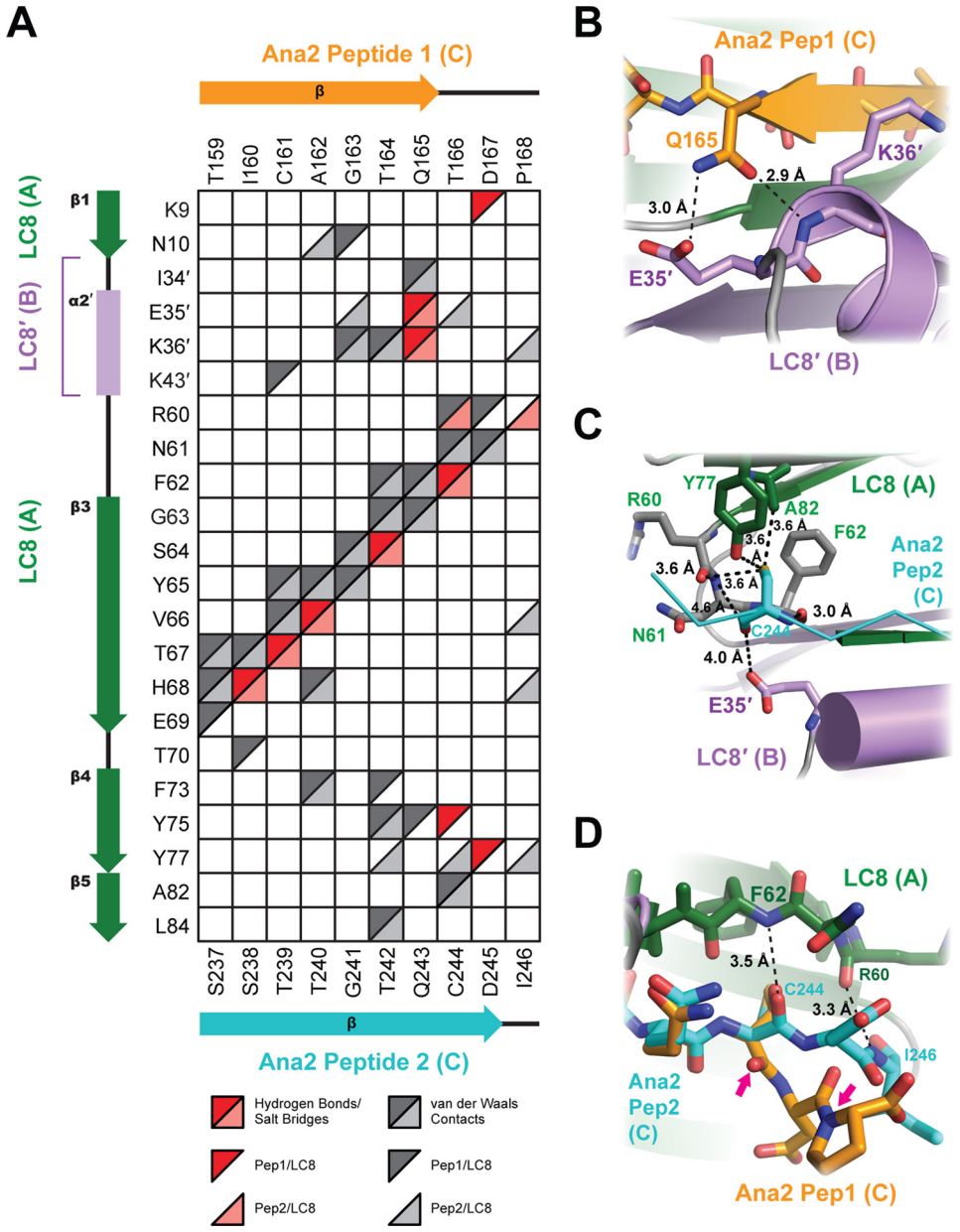

FIGURE 4. **Ana2 LC8-binding sites 1 and 2 employ both shared and unique LC8-binding determinants.** *A*, interaction matrix displaying contacts between the LC8 homodimer (*y axis*) and Ana2 pep1 (*orange*; *top x axis*) or Ana2 pep2 (*cyan*, *bottom x axis*). Interactions are presented where atoms are less than or equal to 3.5 Å apart (hydrogen bonds and electrostatic interactions; shown in *red* for pep1 and *pink* for pep2) and 4.5 Å apart (van der Waals contacts; shown in *dark gray* for pep1 and *light gray* for pep2). *Boxes completely filled in* reflect similar LC8 interaction modes with each peptide, whereas those *boxes* that are *half-filled* indicate unique, peptide-specific interactions. *B*, conserved Gln^{165} of Ana2 pep1 forms hydrogen bonds to LC8′ residues $Glu^{35'}$ and $Lys^{36'}$. *C*, Cys^{244} of Ana2 pep2 forms an electrostatic interaction with LC8 residue Arg^{60}. *D*, the Ana2 pep2 (*cyan*) C-terminal region forms extensive backbone hydrogen bonds with LC8 and is positioned differently than Ana2 pep1 (*orange*), which has been overlaid on the LC8-Ana2 pep2 structure for comparative purposes. In contrast to the Ana2 pep2 Cys^{244} backbone carbonyl and the Ile^{246} backbone amide that interact with LC8 Phe^{62} and Arg^{60}, respectively, the comparable Ana2 pep1 determinants (indicated with *magenta arrows*) are splayed and rotated away from LC8.

Ana2 Employs a Unique Tandem Set of LC8 Binding Motifs—LC8 targets vary widely in their binding affinity and motif composition, both within and beyond the canonical $K^{-3}X^{-2}T^{-1}Q^{0}T^{1}$ or $G^{-2}I^{-1}Q^{0}V^{1}D^{2}$ sequence motifs. Interestingly, both Ana2 LC8 binding motifs combine features from each canonical motif (pep1, $A^{-3}G^{-2}T^{-1}Q^{0}T^{1}D^{2}$; pep2, $T^{-3}G^{-2}T^{-1}Q^{0}C^{1}D^{2}$). Both Ana2 LC8 sites have threonine residues at the −1-position, as found in the $K^{-3}X^{-2}T^{-1}Q^{0}T^{1}$ motif, and both have glycine and aspartate residues at the −2- and +2-positions, as found in the $G^{-2}I^{-1}Q^{0}V^{1}D^{2}$ motif. Neither Ana2 site employs a basic residue at the −3-position, which is often seen in high-affinity LC8 interactors (46), including Nek9 (a kinase that regulates mitotic spindle formation and chromosome separation) (47) and the dynein intermediate chain (DIC; a dynein motor complex component used in cargo recognition) (36) (Fig. 5, *A–C*). Both Nek9 and DIC LC8 target sites contain a lysine at the −3-position (K_{-3}) that interacts with the LC8 D12′ side chain carboxyl group and promotes relatively strong LC8-binding interactions (K_D values on the order of 0.1–0.2 μM) (36, 47) (Fig. 5, *B* and *C*). Ana2 sites 1 and 2 contain an alanine and threonine, respectively, at position −3 that do not

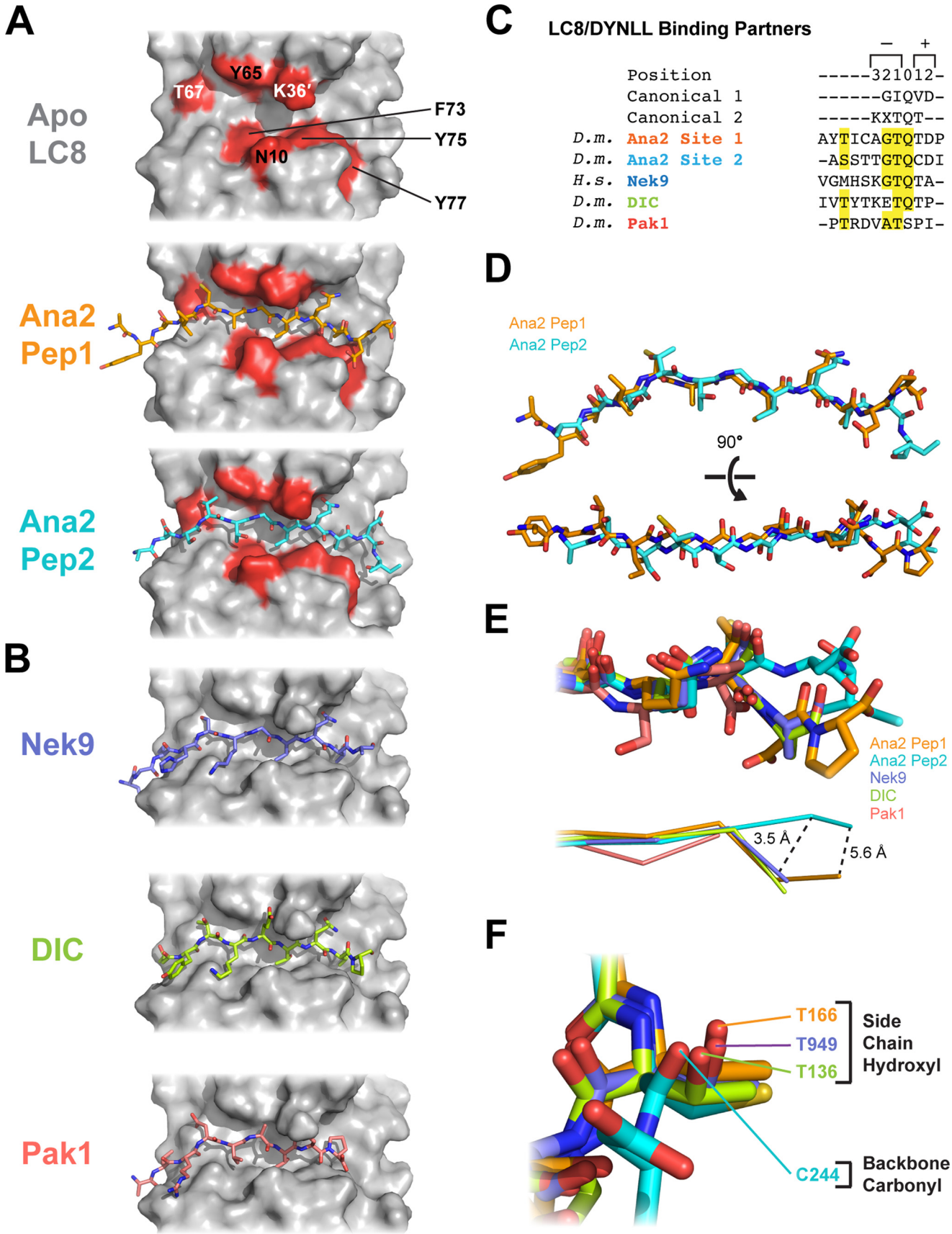
A
Apo LC8
T67
Y65
K36′
N10
F73
Y75
Y77
Ana2 Pep1
Ana2 Pep2
B
Nek9
DIC
Pak1
C
LC8/DYNLL Binding Partners
Position -----321012-
Canonical 1 ------GIQVD-
Canonical 2 -----KXTQT--
D.m. Ana2 Site 1 AYTICAGTQTDP
D.m. Ana2 Site 2 -ASSTTGTQCDI
H.s. Nek9 VGMHSKGTQTA-
D.m. DIC IVTYTKETQTP-
D.m. Pak1 -PTRDVATSPI-
D
Ana2 Pep1
Ana2 Pep2
90°
E
Ana2 Pep1
Ana2 Pep2
Nek9
DIC
Pak1
3.5 Å
5.6 Å
F
T166
T949
T136
Side Chain Hydroxyl
C244
Backbone Carbonyl

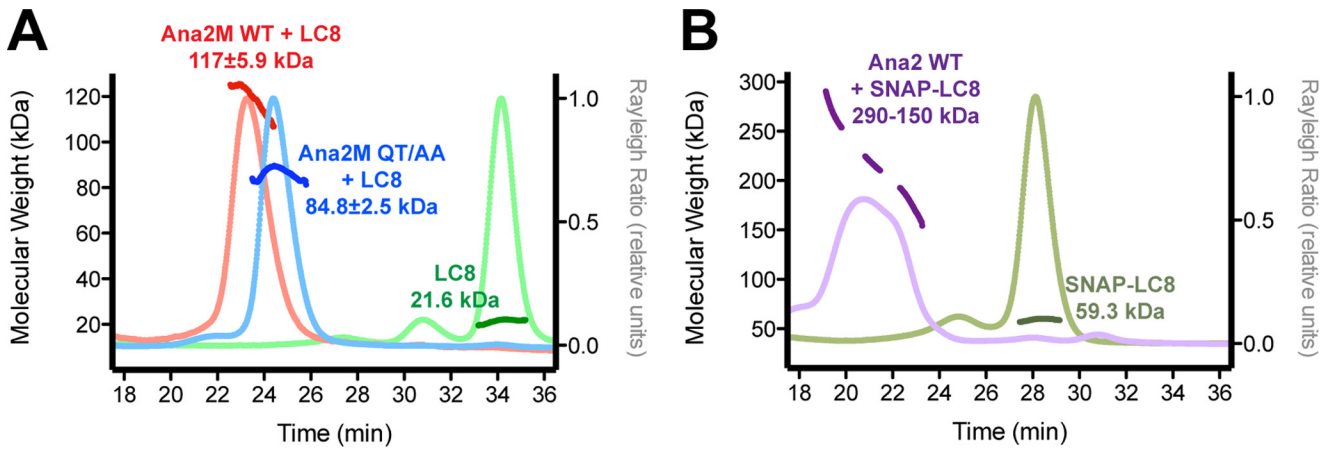

FIGURE 6. **SEC-MALS of Ana2M co-purified with LC8 shows a stable complex corresponding to $LC8_8$-$Ana2M_4$.** Purified Ana2M (residues 156–251, 11 kDa) remained soluble only when co-purified with excess LC8 and behaved as a single species throughout the purification, which included affinity tag chromatography followed by two sizing columns. *A*, detection of the LC8-Ana2M complex on a sizing column coupled with multiangle static light scattering shows a single peak (*pink trace*; Rayleigh ratio) at 117 ± 5.9 kDa (*red*; molecular weight measurement). The same experiments with a Q^0T^1 to A^0A^1 mutation show a single peak (*light blue* trace; Rayleigh ratio) at 84.8 ± 2.5 kDa (*dark blue trace*; molecular weight measurement). LC8 alone elutes as a dimer with a mass of 21.6 kDa (*dark green trace*; molecular weight measurement). *B*, SNAP-LC8 elutes as a single species (*light green trace*; Rayleigh ratio) at 59.3 kDa (*dark green traces*), corresponding to a dimer. Co-purification of SNAP-LC8 with Ana2M yielded a complex that eluted from the size exclusion column in a broad peak, with a shoulder characteristic of complex dissociation (*light purple trace*, Rayleigh ration). Experimentally determined molecular weight across the broad peak indicated complexes of varying size, ranging from 290 to 150 kDa (*dark purple traces*; different parts of the peak were integrated to determine the contributing sizes). All experiments are consistent with the formation of a stable $LC8_8$-$Ana2M_4$ complex.

engage the D12′ side chain carboxyl (Fig. 5*A*). At the −3-position, Pak1 (a kinase that regulates cell motility and, together with LC8, plays a role in cancer transformation (48)) is an interesting point of comparison. Pak1 contains the non-canonical LC8 binding sequence $V^{-3}A^{-2}T^{-1}S^0P^1I^2$ and has the weakest affinity for LC8 (K_D of 42 μM) of the peptides we used for comparison. Like both Ana2 peptides, Pak1 employs a non-charged residue at the −3-position, but similar to the −3 lysine in Nek9 and DIC, positionally equivalent aliphatic side chain determinants are used to engage LC8, highlighting the ability of LC8 to accept side chain variability at the −3-position.

We next examined how the conformations of Ana2 pep1 and pep2 compared with other LC8 binding peptides by aligning LC8-peptide complex structures (Fig. 5, *D–F*). Ana2 pep1 aligns well with other LC8 binding peptides, including Nek9, DIC, and Pak1 (Fig. 5*E*). However, the C-terminal region of Ana2 pep2 departs from this common LC8-bound architecture. The aforementioned Ana2 pep2 cysteine, Cys^{244}, at position +1 is angled into the LC8 peptide-binding groove, effectively positioning the peptide's C-terminal region closer to the LC8 homodimer. In contrast, Ana2 pep1, Nek9, DIC, and Pak1, each of which has a threonine at position +1, splay away from the LC8 dimer, with their C-terminal regions positioned ~3–5 Å from the comparative location of Ana2 pep2 (Fig. 5*E*). Underlying the differential position of Ana2 pep2 is comparative placement of the Cys^{244} backbone carbonyl in the same location of the threonine (Thr^1) side chain hydroxyl as found in Ana2 pep1, Nek9, and DIC (Fig. 5*F*).

LC8 Mediates the Solubility and Oligomerization State of Ana2M—Multiple attempts to express various Ana2 constructs containing either or both of the LC8 binding sites yielded insoluble protein, making it difficult to study the oligomeric state of Ana2 in the absence of LC8. However, co-purification of Ana2M (residues 156–251, encompassing both LC8 binding sites and a central predicted helical domain; Fig. 1*B*) and LC8 yielded a stable, soluble complex that could be purified via the His_6 affinity tag of LC8 followed by size exclusion chromatography. The canonical role of LC8 as a dimerization "hub" led us to predict that the purified LC8-Ana2M complex would form a heterohexamer, with two Ana2M chains forming a central coiled-coil flanked at either end by LC8 homodimers. To experimentally determine the Ana2M-LC8 complex's mass and stoichiometry, we analyzed the complex using SEC-MALS.

As reported previously (29), purified LC8 eluted primarily as a dimer (Fig. 6*A*, *light green trace* indicating the Rayleigh ratio) with a mass of 21.6 kDa (Fig. 6*A*, *dark green trace* indicating the molecular weight). Surprisingly, Ana2M-LC8 formed a stable complex with a mass of 117.1 ± 5.9 kDa (average of four experiments from two independent protein purifications; Fig. 6*A*, *red traces*). This is approximately twice the mass an $Ana2M_2$-$LC8_4$ heterohexamer would form (68 kDa). Adding excess purified LC8 to the Ana2M-LC8 complex did not shift or increase the

FIGURE 5. **The two LC8 binding sites of Ana2 differentially bind LC8.** *A*, a comparison of the LC8 target-binding site among the apo, Ana2 pep1-bound, and Ana2 pep2-bound LC8 structures. Several LC8 residues within the binding pocket show conformational change upon binding peptides and are *colored red*: Asn^{10}, Tyr^{65}, Thr^{67}, Phe^{73}, Tyr^{75}, Tyr^{77}, and $Lys^{36'}$. *B*, comparative panel showing the positioning of other peptides bound to *Drosophila* LC8: Nek9 (Protein Data Bank entry 3ZKE) (47), DIC (Protein Data Bank entry 2PG1) (36), and Pak1 (Protein Data Bank entry 3DVP) (48). *C*, alignment of Ana2 peptides with Nek9, DIC, and Pak1 as well as the canonical binding motifs $G^{-2}I^{-1}Q^0V^1D^2$ and $K^{-3}X^{-2}T^{-1}Q^0T^1$. Conservation is shown in *yellow*, contoured to ≥70% similarity. *D*, Ana2 peptides 1 and 2 superimposed after aligning their respective, bound LC8 homodimers (not shown), viewed in two orientations. *E*, comparisons of the Ana2 peptides with Nek9 (*periwinkle*), DIC (*lime*), and Pak1 (*salmon*) peptides show that although relative positions of the side chains are conserved, the Ana2 pep2 C terminus uniquely bends toward the LC8 homodimer. *Top*, *stick diagram*; *bottom*, *Cα trace*. Measurements of the pep2 backbone show a 3.5 and 5.6-Å positional shift at the +1 and +2 Cα positions, respectively, for Ana2 pep2 *versus* Ana2 pep1. *F*, *zoom view* of the peptides at position +1 reveals the mechanism of the Ana2 pep2 Cys^{244} shift; the same position usually occupied by a +1-position threonine side chain hydroxyl is instead occupied by the Ana2 Cys^{244} backbone carbonyl group. This effectively positions the peptide deeper into the LC8 binding pocket.

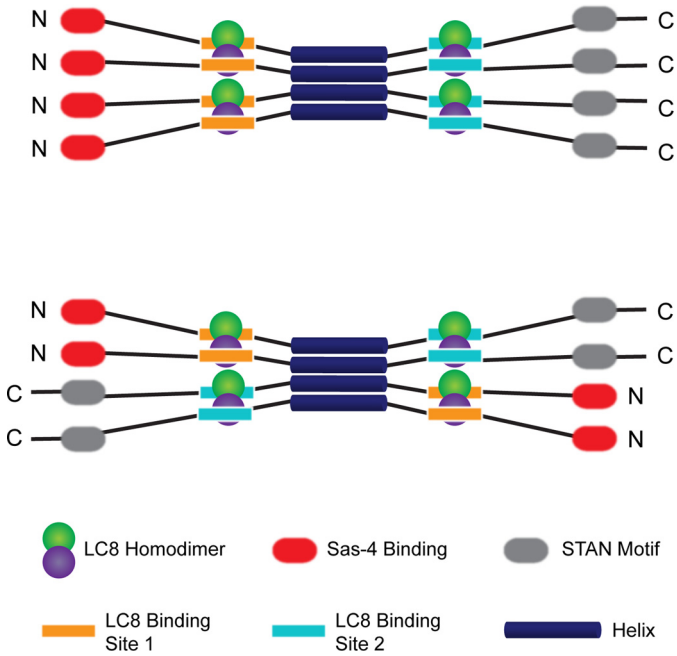

FIGURE 7. **A proposed model of LC8-mediated Ana2 oligomerization.** Our data indicate the formation of an $LC8_8$-$Ana2_4$ complex, which may have implications for the role of Ana2 in centriole duplication by clustering multiple Sas-4-binding (*red ellipses*) and Sas-6-binding (*gray ellipses*) domains. Each LC8 homodimer locally mediates parallel dimerization of Ana2. The model, as presented, portrays the central, predicted α-helix as a tetramerization domain. Whether this domain forms a tetrameric four-helix bundle remains to be determined, but it is presented as a parallel four-helix bundle (*above*) and an antiparallel four-helix bundle (*below*).

mass of the eluted complex but yielded a second peak that eluted later with an experimentally determined mass of 21 kDa, correlating with excess LC8 homodimers (data not shown). These results led us to postulate the existence of an LC8-mediated Ana2M tetramer comprising four Ana2M molecules and four LC8 homodimers ($Ana2M_4$-$LC8_8$; Fig. 7).

To test our predicted stoichiometry, we reasoned that mutating the first LC8 binding site of Ana2 to compromise LC8 binding would result in an $Ana2M_4$-$LC8_4$ complex with a corresponding mass of 90.8 kDa. We mutated the first LC8 binding site of Ana2M (Q165A and T166A or "QT/AA") and co-purified the $Ana2M_{QT/AA}$-LC8 complex, noting that the second LC8-binding site was sufficient for LC8-mediated Ana2M solubilization. The $Ana2M_{QT/AA}$-LC8 mutant retained its solubility and showed an excess of unbound LC8 during size exclusion chromatography. In accordance with forming an $Ana2M_4$-$LC8_4$ heterooctomer (predicted mass of 90.8 kDa), the complex had an apparent mass of 84.8 ± 2.5 kDa (Fig. 6*A*, *blue traces*).

In our experiments, Ana2M and LC8 were approximately the same mass (11.4 and 11.3 kDa, respectively), making it difficult to determine the relative contribution of LC8 and Ana2M to the complex. To independently confirm the composition of the proposed $Ana2M_4$-$LC8_8$ complex, we purified an N-terminally SNAP-tagged LC8 (monomer mass, 30 kDa) alone and in complex with Ana2M. The SNAP tag served the sole purpose of increasing the mass of the LC8 construct to see how this change in turn altered the mass of the Ana2M-LC8 complex. An $Ana2M_4$-SNAP-$LC8_8$ complex would have a mass of 286 kDa. SNAP-LC8 was expressed with an N-terminal His tag and behaved similar to wild-type LC8 throughout purification. Purified SNAP-LC8 eluted from the SEC-MALS column as a homodimer with an apparent mass of 59.3 kDa, indicative that the SNAP tag does not interfere with LC8 dimerization (Fig. 6*B*, *dark green trace*). Ana2M co-purified with SNAP-LC8, suggesting that SNAP-LC8 retained target-binding capabilities. The Ana2M-SNAP-LC8 complex eluted broadly from the SEC-MALS column with experimentally determined masses ranging from 290 kDa (early portion of the elution peak) to 150 kDa (later portion of the elution peak) (Fig. 6*B*, *purple trace*). The early portion of the elution peak mass correlates with an $Ana2M_4$-SNAP-$LC8_8$ complex, whereas the 150 kDa shoulder suggested that the SNAP tag may sterically hinder Ana2 tetramerization, yielding a $Ana2M_2$-SNAP-$LC8_4$ subspecies.

DISCUSSION

Ana2 is an integral component of the centriole duplication pathway, but how it works with Sas-6 and Sas-4 and whether LC8 plays a role in this pathway remain to be determined. The Sas-6 dimer interactions that facilitate cartwheel formation are very weak (K_D of >100 μM), making it unlikely that Sas-6 could spontaneously build cartwheels in a cellular context at endogenous levels. Additionally, Sas-6 overexpression promotes centriole amplification only when Ana2 is co-overexpressed, suggesting that Ana2 plays a supporting role in enhancing Sas-6 oligomerization and cartwheel formation (17). One mechanism by which Ana2 could promote Sas-6 oligomerization would be if Ana2 itself were oligomeric. This idea is supported by recent evidence that Ana2 binds LC8, a dynein light chain that plays a ubiquitous role as a dimerization machine (24). Our work provides insight into the Ana2-LC8 quaternary structure and establishes a foundation upon which the Ana2 tetramer's avidity effects on Sas-6 oligomerization can be investigated.

We have identified two LC8 binding sites in Ana2, conserved within the *Drosophila* genus, that flank a central domain with predicted helical structure (Fig. 1*E*). Although the exact binding sites are not apparent in other metazoan species, the presence of a central predicted coiled-coil is conserved across Ana2 orthologs from *C. elegans* Sas-5 to human STIL and suggests a role in oligomerization. This is supported by a report that the *C. elegans* Sas-5 N-terminal region (containing the central predicted coiled-coil) forms a tetramer in solution (49). Although Sas-5 tetramerization *in vitro* is not LC8-dependent, its oligomeric state parallels the LC8-dependent tetramerization that we observe with Ana2.

Dynein light chains often bind targets proximal to an endogenous oligomerization domain, potentiating target dimerization. Both of the Ana2 LC8-binding sites are an amalgam of the canonical $K^{-3}X^{-2}T^{-1}Q^0T^1$ and $G^{-2}I^{-1}Q^0V^1D^2$ LC8-binding motifs. Using ITC, we have shown that Ana2 pep1 binds LC8 with micromolar affinity (K_D = 1.1 μM). Our crystal structure of LC8 bound to Ana2 pep1 shows an $LC8_2$-$Ana2\ pep1_2$ binding mode, with the Ana2 pep1 canonical TQT sequence contributing key binding determinants.

Our second identified LC8-binding site (Ana2 site 2, pep2) flanks the central helical domain's C-terminal region and is composed of the sequence $T^{-3}G^{-2}T^{-1}Q^0C^1D^2$. Ana2 pep2 binds LC8 with lower affinity (K_D = 13 μM) than Ana2 pep1.

Our crystal structure of LC8 bound to Ana2 pep2 also has an $LC8_2$-Ana2 $pep2_2$ binding mode. Interestingly, Ana2 pep2 adopts a unique architecture when bound to LC8 that contrasts with other LC8-peptide structures. The Ana2 pep2 Cys^{244} at position +1 is positioned deeper into the LC8 binding groove. The affinities we report for the LC8-Ana2 peptide interactions probably underestimate the stability of the biological complex involving full-length Ana2 and LC8. Because our solution studies support interactions between LC8 homodimers and a tetrameric Ana2M region, we anticipate that avidity effects will increase the complex's stability beyond the affinities we report for LC8 and Ana2 pep1 and pep2. This is consistent with the finding that a stable Ana2-LC8 complex can be extracted from *Drosophila* cell lysate (24). We note that within the genus *Drosophila*, the two segments that bridge the predicted central coiled-coil with the two flanking LC8 binding sites are not conserved in sequence or length. We predict that these segments serve as general spacers that link the LC8 binding sites to the Ana2 coiled-coil oligomerization domain and maintain a general length that enables LC8 homodimers to bind and potentiate Ana2 oligomerization without sterically compromising coiled-coil formation.

Our data support a model in which LC8 stabilizes an Ana2 tetramer (Fig. 7). An Ana2 tetramer may spatially arrange its conserved C-terminal STAN motifs to interact with Sas-6 and promote the Sas-6 oligomerization that underlies centriole cartwheel formation. Our SEC-MALS analysis of the Ana2M-LC8 complex reveals a stable, single-species complex consisting of four Ana2M molecules and eight LC8 molecules ($Ana2M_4$-$LC8_8$). This stable complex was purified over two successive sizing columns, demonstrating its ready formation, and yielded a similar experimental mass in two independent purifications and SEC-MALS assays. Mutating the first Ana2M LC8 binding site as well as adding a SNAP tag to LC8 supported the $Ana2M_4$-$LC8_8$ stoichiometry (Fig. 7).

The Ana2-LC8 interactions that we characterized raise important questions about the role of Ana2 in centriole duplication. Previous work has shown that the C-terminal half of Ana2 binds the N terminus of Sas-6 in *Drosophila* (12), implicating a possible role for the conserved STAN domain of Ana2 in Sas-6 binding. In our model, LC8 binds and stabilizes an Ana2 tetramer that may structurally organize four trans STAN domains at one end of a parallel tetramerization domain or two trans STAN domains at either end of an antiparallel tetramerization domain (Fig. 7). In either configuration, the oligomeric state of Ana2, coupled with its ability to bind Sas-6, is predicted to enhance Sas-6 oligomerization and cartwheel formation. This correlates with cellular studies in which Sas-6 and Ana2 dual overexpression was required for cartwheel formation, suggesting that Ana2 potentiates Sas-6 cartwheel formation, potentially through oligomerization (17). Recent cryotomographic studies of nascent centriole architecture reveal auxiliary protein density connecting the Sas-6-based cartwheel to Sas-4 and the distal microtubule triplets (3). Given the integral role of Ana2 in Sas-6 cartwheel formation as well as evidence that it binds both Sas-6 and Sas-4, Ana2 is a likely candidate for this density. More work is needed to determine if Ana2 can bridge Sas-6 and Sas-4 and whether the LC8-Ana2 interaction plays a role in this Ana2 function, as it does in neuroblast asymmetric cell division. Our work outlines the structural basis of the LC8-Ana2 interaction, with implications for its role in Ana2 structure and function at the centriole.

REFERENCES

1. Bornens, M. (2012) The centrosome in cells and organisms. *Science* **335,** 422–426
2. Gönczy, P. (2012) Towards a molecular architecture of centriole assembly. *Nat. Rev. Mol. Cell Biol.* **13,** 425–435
3. Guichard, P., Hachet, V., Majubu, N., Neves, A., Demurtas, D., Olieric, N., Fluckiger, I., Yamada, A., Kihara, K., Nishida, Y., Moriya, S., Steinmetz, M. O., Hongoh, Y., and Gönczy, P. (2013) Native architecture of the centriole proximal region reveals features underlying its 9-fold radial symmetry. *Curr. Biol.* **23,** 1620–1628
4. Tsou, M. F., and Stearns, T. (2006) Mechanism limiting centrosome duplication to once per cell cycle. *Nature* **442,** 947–951
5. Pelletier, L., O'Toole, E., Schwager, A., Hyman, A. A., and Müller-Reichert, T. (2006) Centriole assembly in *Caenorhabditis elegans*. *Nature* **444,** 619–623
6. Habedanck, R., Stierhof, Y. D., Wilkinson, C. J., and Nigg, E. A. (2005) The Polo kinase Plk4 functions in centriole duplication. *Nat. Cell Biol.* **7,** 1140–1146
7. Lettman, M. M., Wong, Y. L., Viscardi, V., Niessen, S., Chen, S. H., Shiau, A. K., Zhou, H., Desai, A., and Oegema, K. (2013) Direct binding of SAS-6 to ZYG-1 recruits SAS-6 to the mother centriole for cartwheel assembly. *Dev. Cell* **25,** 284–298
8. van Breugel, M., Hirono, M., Andreeva, A., Yanagisawa, H. A., Yamaguchi, S., Nakazawa, Y., Morgner, N., Petrovich, M., Ebong, I. O., Robinson, C. V., Johnson, C. M., Veprintsev, D., and Zuber, B. (2011) Structures of SAS-6 suggest its organization in centrioles. *Science* **331,** 1196–1199
9. Kitagawa, D., Vakonakis, I., Olieric, N., Hilbert, M., Keller, D., Olieric, V., Bortfeld, M., Erat, M. C., Flückiger, I., Gönczy, P., and Steinmetz, M. O. (2011) Structural basis of the 9-fold symmetry of centrioles. *Cell* **144,** 364–375
10. Hilbert, M., Erat, M. C., Hachet, V., Guichard, P., Blank, I. D., Flückiger, I., Slater, L., Lowe, E. D., Hatzopoulos, G. N., Steinmetz, M. O., Gönczy, P., and Vakonakis, I. (2013) Caenorhabditis elegans centriolar protein SAS-6 forms a spiral that is consistent with imparting a ninefold symmetry. *Proc. Natl. Acad. Sci. U.S.A.* **110,** 11373–11378
11. Goshima, G., Wollman, R., Goodwin, S. S., Zhang, N., Scholey, J. M., Vale, R. D., and Stuurman, N. (2007) Genes required for mitotic spindle assembly in *Drosophila* S2 cells. *Science* **316,** 417–421
12. Stevens, N. R., Dobbelaere, J., Brunk, K., Franz, A., and Raff, J. W. (2010) *Drosophila* Ana2 is a conserved centriole duplication factor. *J. Cell Biol.* **188,** 313–323
13. Cottee, M. A., Muschalik, N., Wong, Y. L., Johnson, C. M., Johnson, S., Andreeva, A., Oegema, K., Lea, S. M., Raff, J. W., and van Breugel, M. (2013) Crystal structures of the CPAP/STIL complex reveal its role in centriole assembly and human microcephaly. *Elife* **2,** e01071
14. Hatzopoulos, G. N., Erat, M. C., Cutts, E., Rogala, K. B., Slater, L. M., Stansfeld, P. J., and Vakonakis, I. (2013) Structural analysis of the G-box domain of the microcephaly protein CPAP suggests a role in centriole architecture. *Structure* **21,** 2069–2077
15. Leidel, S., Delattre, M., Cerutti, L., Baumer, K., and Gönczy, P. (2005) SAS-6 defines a protein family required for centrosome duplication in *C. elegans* and in human cells. *Nat. Cell Biol.* **7,** 115–125
16. Qiao, R., Cabral, G., Lettman, M. M., Dammermann, A., and Dong, G. (2012) SAS-6 coiled-coil structure and interaction with SAS-5 suggest a regulatory mechanism in *C. elegans* centriole assembly. *EMBO J.* **31,** 4334–4347
17. Stevens, N. R., Roque, H., and Raff, J. W. (2010) DSas-6 and Ana2 coassemble into tubules to promote centriole duplication and engagement. *Dev. Cell* **19,** 913–919
18. Arquint, C., Sonnen, K. F., Stierhof, Y-D., and Nigg, E. A. (2012) Cell-cycle-regulated expression of STIL controls centriole number in human cells. *J. Cell Sci.* **125,** 1342–1352

19. Aplan, P. D., Lombardi, D. P., and Kirsch, I. R. (1991) Structural characterization of SIL, a gene frequently disrupted in T-cell acute lymphoblastic leukemia. *Mol. Cell Biol.* **11,** 5462–5469
20. Izraeli, S., Colaizzo-Anas, T., Bertness, V. L., Mani, K., Aplan, P. D., and Kirsch, I. R. (1997) Expression of the SIL gene is correlated with growth induction and cellular proliferation. *Cell Growth Differ.* **8,** 1171–1179
21. Erez, A., Perelman, M., Hewitt, S. M., Cojacaru, G., Goldberg, I., Shahar, I., Yaron, P., Muler, I., Campaner, S., Amariglio, N., Rechavi, G., Kirsch, I. R., Krupsky, M., Kaminski, N., and Izraeli, S. (2004) Sil overexpression in lung cancer characterizes tumors with increased mitotic activity. *Oncogene* **23,** 5371–5377
22. Basto, R., Brunk, K., Vinadogrova, T., Peel, N., Franz, A., Khodjakov, A., and Raff, J. W. (2008) Centrosome amplification can initiate tumorigenesis in flies. *Cell* **133,** 1032–1042
23. Kumar, A., Girimaji, S. C., Duvvari, M. R., and Blanton, S. H. (2009) Mutations in STIL, encoding a pericentriolar and centrosomal protein, cause primary microcephaly. *Am. J. Hum. Genet.* **84,** 286–290
24. Wang, C., Li, S., Januschke, J., Rossi, F., Izumi, Y., Garcia-Alvarez, G., Gwee, S. S., Soon, S. B., Sidhu, H. K., Yu, F., Matsuzaki, F., Gonzalez, C., and Wang, H. (2011) An Ana2/Ctp/Mud complex regulates spindle orientation in *Drosophila* neuroblasts. *Dev. Cell* **21,** 520–533
25. Barbar, E. (2008) Dynein light chain LC8 is a dimerization hub essential in diverse protein networks. *Biochemistry* **47,** 503–508
26. Lei, K., and Davis, R. J. (2003) JNK phosphorylation of Bim-related members of the Bcl2 family induces Bax-dependent apoptosis. *Proc. Natl. Acad. Sci. U.S.A.* **100,** 2432–2437
27. Liang, J., Jaffrey, S. R., Guo, W., Snyder, S. H., and Clardy, J. (1999) Structure of the PIN/LC8 dimer with a bound peptide. *Nat. Struct. Biol.* **6,** 735–740
28. Chaudhury, A., Rao, Y. M., and Goyal, R. K. (2008) PIN/LC8 is associated with cytosolic but not membrane-bound nNOS in the nitrergic varicosities of mice gut: implications for nitrergic neurotransmission. *Am. J. Physiol. Gastrointest. Liver Physiol.* **295,** G442–G451
29. Romes, E. M., Tripathy, A., and Slep, K. C. (2012) Structure of a yeast Dyn2-Nup159 complex and molecular basis for dynein light chain-nuclear pore interaction. *J. Biol. Chem.* **287,** 15862–15873
30. Nyarko, A., Song, Y., Nováček, J., Žídek, L., and Barbar, E. (2013) Multiple recognition motifs in nucleoporin Nup159 provide a stable and rigid Nup159-Dyn2 assembly. *J. Biol. Chem.* **288,** 2614–2622
31. Purohit, A., Tynan, S. H., Vallee, R., and Doxsey, S. J. (1999) Direct interaction of pericentrin with cytoplasmic dynein light intermediate chain contributes to mitotic spindle organization. *J. Cell Biol.* **147,** 481–492
32. Navarro, C., Puthalakath, H., Adams, J. M., Strasser, A., and Lehmann, R. (2004) Egalitarian binds dynein light chain to establish oocyte polarity and maintain oocyte fate. *Nat. Cell Biol.* **6,** 427–435
33. Asthana, J., Kuchibhatla, A., Jana, S. C., Ray, K., and Panda, D. (2012) Dynein light chain 1 (LC8) association enhances microtubule stability and promotes microtubule bundling. *J. Biol. Chem.* **287,** 40793–40805
34. Nyarko, A., and Barbar, E. (2011) Light chain-dependent self-association of dynein intermediate chain. *J. Biol. Chem.* **286,** 1556–1566
35. Benison, G., Karplus, P. A., and Barbar, E. (2007) Structure and dynamics of LC8 complexes with KXTQT-motif peptides: Swallow and dynein intermediate chain compete for a common site. *J. Mol. Biol.* **371,** 457–468
36. Williams, J. C., Roulhac, P. L., Roy, A. G., Vallee, R. B., Fitzgerald, M. C., and Hendrickson, W. A. (2007) Structural and thermodynamic characterization of a cytoplasmic dynein light chain-intermediate chain complex. *Proc. Natl. Acad. Sci. U.S.A.* **104,** 10028–10033
37. Stuchell-Brereton, M. D., Siglin, A., Li, J., Moore, J. K., Ahmed, S., Williams, J. C., and Cooper, J. A. (2011) Functional interaction between dynein light chain and intermediate chain is required for mitotic spindle positioning. *Mol. Biol. Cell* **22,** 2690–2701
38. Otwinowski, Z., and Minor, W. (1997) Processing of x-ray diffraction data collected in oscillation mode. *Methods Enzymol.* **276,** 307–326
39. Adams, P. D., Afonine, P. V., Bunkóczi, G., Chen, V. B., Davis, I. W., Echols, N., Headd, J. J., Hung, L. W., Kapral, G. J., Grosse-Kunstleve, R. W., McCoy, A. J., Moriarty, N. W., Oeffner, R., Read, R. J., Richardson, D. C., Richardson, J. S., Terwilliger, T. C., and Zwart, P. H. (2010) PHENIX: a comprehensive Python-based system for macromolecular structure solution. *Acta Crystallogr. D Biol. Crystallogr.* **66,** 213–221
40. Emsley, P., Lohkamp, B., Scott, W. G., and Cowtan, K. (2010) Features and development of Coot. *Acta Crystallogr. D Biol. Crystallogr.* **66,** 486–501
41. Brünger, A. T. (1992) Free *R* value: a novel statistical quantity for assessing the accuracy of crystal structures. *Nature* **355,** 472–475
42. Wyatt, P. J. (1993) Light scattering and the absolute characterization of macromolecules. *Anal. Chim. Acta* 10.1016/0003-2670(93)80373-S
43. Rao, L., Romes, E. M., Nicholas, M. P., Brenner, S., Tripathy, A., Gennerich, A., and Slep, K. C. (2013) The yeast dynein Dyn2-Pac11 complex is a dynein dimerization/processivity factor: structural and single-molecule characterization. *Mol. Biol. Cell* **24,** 2362–2377
44. Rapali, P., Szenes, Á., Radnai, L., Bakos, A., Pál, G., and Nyitray, L. (2011) DYNLL/LC8: a light chain subunit of the dynein motor complex and beyond. *FEBS J.* **278,** 2980–2996
45. Benison, G., Karplus, P. A., and Barbar, E. (2008) The interplay of ligand binding and quaternary structure in the diverse interactions of dynein light chain LC8. *J. Mol. Biol.* **384,** 954–966
46. Rapali, P., Radnai, L., Süveges, D., Harmat, V., Tölgyesi, F., Wahlgren, W. Y., Katona, G., Nyitray, L., and Pál, G. (2011) Directed evolution reveals the binding motif preference of the LC8/DYNLL hub protein and predicts large numbers of novel binders in the human proteome. *PLoS One* **6,** e18818
47. Gallego, P., Velazquez-Campoy, A., Regué, L., Roig, J., and Reverter, D. (2013) Structural analysis of the regulation of the DYNLL/LC8 binding to Nek9 by phosphorylation. *J. Biol. Chem.* **288,** 12283–12294
48. Lightcap, C. M., Sun, S., Lear, J. D., Rodeck, U., Polenova, T., and Williams, J. C. (2008) Biochemical and structural characterization of the Pak1-LC8 interaction. *J. Biol. Chem.* **283,** 27314–27324
49. Shimanovskaya, E., Qiao, R., Lesigang, J., and Dong, G. (2013) The SAS-5 N-terminal domain is a tetramer, with implications for centriole assembly in *C. elegans*. *Worm* **2,** e25214
50. Dzhindzhev, N. S., Yu, Q. D., Weiskopf, K., Tzolovsky, G., Cunha-Ferreira, I., Riparbelli, M., Rodrigues-Martins, A., Bettencourt-Dias, M., Callaini, G., and Glover, D. M. (2010) Asterless is a scaffold for the onset of centriole assembly. *Nature* **467,** 714–718
51. Slevin, L. K., Nye, J., Pinkerton, D. C., Buster, D. W., Rogers, G. C., and Slep, K. C. (2012) The structure of the Plk4 cryptic polo box reveals two tandem polo boxes required for centriole duplication. *Structure* **20,** 1905–1917
52. Puklowski, A., Homsi, Y., Keller, D., May, M., Chauhan, S., Kossatz, U., Grünwald, V., Kubicka, S., Pich, A., Manns, M. P., Hoffmann, I., Gönczy, P., and Malek, N. P. (2011) The SCF-FBXW5 E3-ubiquitin ligase is regulated by Plk4 and targets HsSAS-6 to control centrosome duplication. *Nat. Cell Biol.* **13,** 1004–1009
53. Lerit, D. A., and Rusan, N. M. (2013) PLP inhibits the activity of interphase centrosomes to ensure their proper segregation in stem cells. *J. Cell Biol.* **202,** 1013–1022